Measurement of the Neutron Lifetime Using a Proton Trap

M. S. Dewey, D. M. Gilliam, and J. S. Nico

National Institute of Standards and Technology, Gaithersburg, Maryland 20899, USA

F. E. Wietfeldt

Tulane University, New Orleans, Louisiana 70118, USA

X. Fei and W. M. Snow

Indiana University, Bloomington, Indiana 47408, USA

G. L. Greene

University of Tennessee/Oak Ridge National Laboratory, Knoxville, Tennessee 37996, USA

J. Pauwels, R. Eykens, A. Lamberty, and J. Van Gestel

European Commission, Joint Research Centre, Institute for Reference Materials and Measurements, 2440 Geel, Belgium
(Received 5 May 2003; published 10 October 2003)

We report a new measurement of the neutron decay lifetime by the absolute counting of in-beam neutrons and their decay protons. Protons were confined in a quasi-Penning trap and counted with a silicon detector. The neutron beam fluence was measured by capture in a thin ^{6}LiF foil detector with known absolute efficiency. The combination of these simultaneous measurements gives the neutron lifetime: $\tau_n = (886.8 \pm 1.2[\text{stat}] \pm 3.2[\text{syst}])$ s. The systematic uncertainty is dominated by uncertainties in the mass of the ^{6}LiF deposit and the ^{6}Li(n, t) cross section. This is the most precise measurement of the neutron lifetime to date using an in-beam method.

Precision measurements of neutron beta decay address basic questions in particle physics, astrophysics, and cosmology. As the simplest semileptonic decay system, the free neutron plays a crucial role in understanding the physics of the weak interaction [1]. The current experimental uncertainty in the neutron lifetime dominates the uncertainty in calculating the primordial helium abundance, as a function of baryon density, using big-bang nucleosynthesis [2]. Figure 1 shows a summary of recent neutron lifetime measurements. The four most precise experiments [4,6,7,9] confined ultracold neutrons (UCN) in a bottle; the decay lifetime is determined by counting the neutrons that remain after some elapsed time, with a correction for competing neutron loss mechanisms. Two others [3,8] measured the absolute specific activity of a beam of cold neutrons by counting decay protons. These two classes of experiments encounter very different systematic problems, so a more precise in-beam measurement improves both the precision of τ_n and the robustness of the central value. Note that the in-beam method measures only the neutron decay branch that produces a proton in the final state, while the UCN bottle method measures all decay modes.

Figure 2 shows a sketch of the experimental method. It is based on the method first proposed by Byrne *et al.* and is described in greater detail in previous publications [10]. A proton trap of length L intercepts the entire width of the neutron beam. Neutron decay is observed by trapping and counting decay protons within the trap with an effi-

ciency ϵ_p. The neutron beam is characterized by a velocity dependent fluence rate $I(v)$. The mean number of neutrons inside the trap volume is

$$N_n = L \int_A da I(v) \frac{1}{v}, \qquad (1)$$

where A is the beam cross sectional area, and so the rate $\dot{N}_p$ at which decay protons are detected is

$$\dot{N}_p = \frac{\epsilon_p L}{\tau_n} \int_A da I(v) \frac{1}{v}. \qquad (2)$$

After leaving the trap, the neutron beam passes through a thin foil of ^{6}LiF. The probability for absorbing a neutron
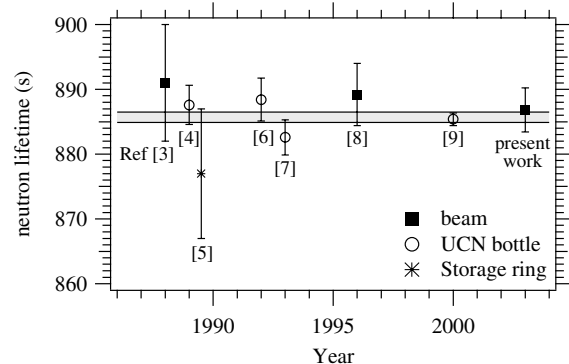

FIG. 1. A comparison of recent neutron lifetime measurements. The shaded band is ± 1 standard deviation of the weighted average, including our result.
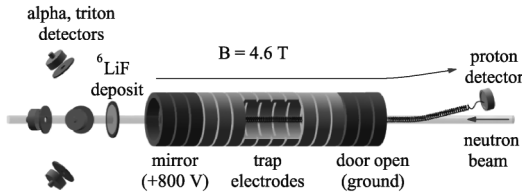
FIG. 2. Schematic representation of the experimental method (not to scale).

in the foil through the ^{6}Li$(n, t)^4$He reaction is inversely proportional to the neutron velocity v. The reaction products, alphas or tritons, are counted by a set of four silicon surface barrier detectors in a well-characterized geometry. We define the efficiency for the neutron detector, ϵ_o, as the ratio of the reaction product rate to the neutron rate incident on the deposit for neutrons with thermal velocity $v_o = 2200$ m/s. The corresponding efficiency for neutrons of other velocities is $\epsilon_o v_o / v$. Therefore, the net reaction product count rate $\dot{N}_\alpha$ is

$$\dot{N}_\alpha = \epsilon_o v_o \int_A da I(v) \frac{1}{v}. \qquad (3)$$

The integrals in Eqs. (2) and (3) are identical; the velocity dependence of the neutron detector efficiency compensates for the fact that the faster neutrons in the beam spend less time in the decay volume. This cancellation is exact given two assumptions: (i) the neutron absorption efficiency in the ^{6}LiF target is exactly proportional to $1/v$ and (ii) the neutron beam intensity and its velocity dependence do not change between the trap and the target. The deviation from the $1/v$ law in the ^{6}Li$(n, t)^4$He cross section at thermal and subthermal energies has been shown to be less than 0.01% [11], and changes in the neutron beam due to decay in flight and residual gas interaction are less than 0.001%. Our only non-negligible correction to Eqs. (2) and (3) is for the finite thickness of the ^{6}LiF foil (+ 5.4 s). Thus we obtain the neutron lifetime τ_n from the experimental quantities $\dot{N}_\alpha/\dot{N}_p$, ϵ_o, ϵ_p, and L.

The experiment was performed at the cold neutron beam line NG6 at the National Institute of Standards and Technology (NIST) Center for Neutron Research. The neutron beam was collimated by two ^{6}LiF apertures. The diameter of the first aperture (C1) was varied from 32 to 51 mm as a systematic check on the effect of the beam diameter on the measured lifetime. The second (C2) had a diameter of 8.4 mm and was not changed. The collimated beam transited a 1 m section of preguide and then entered the vacuum system through a 7.5 mm inner diameter quartz guide tube. After passing through the trap, it traveled 83 cm to the ^{6}LiF deposit. The beam exited the vacuum system through a silicon window and stopped in a thick ^{6}LiF beam dump.

The proton trap was a quasi-Penning trap, composed of 16 annular electrodes, each 18.6-mm long with an inner diameter of 26.0 mm, cut from fused quartz and coated

with a thin layer of gold. Adjacent segments were separated by 3-mm-thick insulating spacers of uncoated fused quartz. The dimensions of each electrode and spacer were measured to a precision of ± 5 μm using a coordinate measuring machine at NIST. Changes in the dimension due to thermal contraction are below the 10^{-4} level for fused quartz. The trap resided in a 4.6 T magnetic field and the vacuum in the trap was maintained below 10^{-9} mbar.

In trapping mode, the three upstream electrodes (the "door") were held at $+800$ V, and a variable number of adjacent electrodes (the "trap") were held at ground potential. The subsequent three electrodes (the "mirror") were held at $+800$ V. We varied the trap length from three to ten electrodes. When a neutron decayed inside the trap, the decay proton was trapped radially by the magnetic field and axially by the electrostatic potential in the door and mirror. After some trapping period, typically 10 ms, the trapped protons were counted. The door electrodes were lowered to ground potential, and a small ramped potential was applied to the trap electrodes to assist the slower protons out the door. The protons were then guided by a 9.5° bend in the magnetic field to the proton detector held at a high negative potential (-27.5 to -32.5 kV). After 76 μs, a time sufficient for all protons to exit the trap, the mirror was lowered to ground potential. This prevented negatively charged particles, which may contribute to instability, from accumulating in any portion of the trap. That state was maintained for 33 μs, after which the door and mirror electrodes were raised again to $+800$ V and another trapping cycle began. Since the detector needed to be enabled only during extraction, the counting background was reduced by the ratio of the trapping time to the extraction time (typically a factor of 125). Figure 3 shows a plot of proton detection time for a typical run.

Protons that were born in the trap (grounded electrode region) were trapped with 100% efficiency. However, protons that were born near the door and mirror (the "end
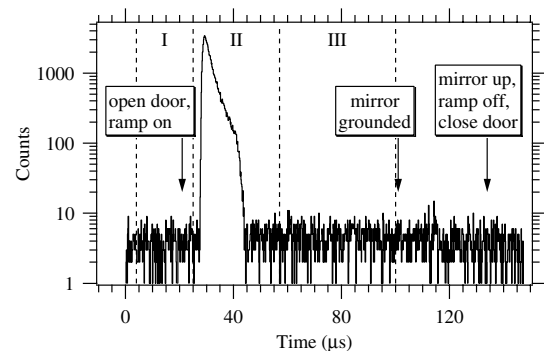

FIG. 3. A typical plot of proton detection time after gating on the detector ($t = 0$). Regions I and III are used to subtract background from the peak region II. After correcting for dead time in the time-to-digital converter, the resulting peak area gives the proton rate $\dot{N}_p$.

regions"), where the electrostatic potential is elevated, were not all trapped. A proton born in the end region was trapped if its initial (at birth) sum of electrostatic potential energy and axial kinetic energy was less than the maximum end potential. This complication caused the effective length L of the trap to be difficult to determine precisely. It is for this reason that we varied the trap length. The shape of the electrostatic potential near the door and mirror was the same for all traps with three to ten grounded electrodes, so the effective length of the end regions, while unknown, was in principle constant. The length of the trap can then be written $L = nl + L_{end}$, where n is the number of grounded electrodes and l is the physical length of one electrode plus an adjacent spacer. L_{end} is an *effective* length of the two end regions; it is proportional to the physical length of the end regions *and* the probability that protons born there will be trapped. From Eqs. (2) and (3) we see that the ratio of proton counting rate to alpha counting rate is then

$$\frac{\dot{N}_p}{\dot{N}_\alpha} = \tau_n^{-1}\left(\frac{\epsilon_p}{\epsilon_0 v_o}\right)(nl + L_{end}). \quad (4)$$

We fit $\dot{N}_p/\dot{N}_\alpha$ as a function of n to a straight line and determine τ_n from the slope, so there is no need to know the value of L_{end}, provided that it was the same for all trap lengths.

Because of the symmetry in the Penning trap's design, L_{end} was approximately equal for all trap lengths. There were two trap-length-dependent effects that broke the symmetry: the gradient in the axial magnetic field, and the divergence of the neutron beam. Each of these effects caused L_{end} to vary slightly with trap length. A detailed Monte Carlo simulation of the experiment, based on the measured and calculated magnetic and electric field inside the trap, was developed in order to correct for these trap nonlinearities. It gave a trap-length dependent correction that lowered the lifetime by 5.3 s.

Surface barrier and passivated ion-implanted planar silicon detectors were used at various times for counting the protons. The proton detectors were large enough so that all protons produced by neutron decay in the collimated beam, defined by C1 and C2, would strike the 19.7-mm-diameter active region after the trap was opened. The detector was optically aligned to the magnetic field axis, and the alignment was verified by scanning with a low energy electron source at the trap's center and with actual neutron decay protons. When a proton hit the active region of the detector, the efficiency for proton detection was less than unity because (i) a proton can lose so much energy in the inactive surface dead layer that it deposits insufficient energy in the active region to be detected, (ii) a proton can be stopped within the dead layer and never reach the active region, and (iii) a proton can backscatter from the dead layer or the active region and deposit insufficient energy. In the first two cases, the proton will definitely not be detected. We denote the

fraction of protons lost in this manner by f_{lost}. In the last case, there is some probability that the backscattered proton will be reflected back to the detector by the electric field and subsequently be detected. We denote the fraction of protons that backscatter but still have some chance for detection by f_{bsc}.

To determine the proton detection efficiency, we ran the experiment with a variety of detectors with different dead layer thicknesses and different acceleration potentials. The fraction of protons lost f_{lost} and the fraction that backscatter f_{bsc} were calculated using the SRIM-2000 Monte Carlo program [12]. We found that f_{lost} varied from $4.0(3) \times 10^{-5}$ to $8.0(6) \times 10^{-3}$, and f_{bsc} from $1.83(13) \times 10^{-3}$ to $2.37(17) \times 10^{-2}$, depending on the detector and acceleration potential. The proton counting rate $\dot{N}_p$ for each run was multiplied by $1 + f_{lost}$ to correct for lost protons. The correction for backscattered protons was not as simple because of the unknown probability for a backscattered proton to return and be detected, so we made an extrapolation of the measured neutron lifetime to zero backscatter fraction (see Fig. 4).

The neutron detector target was a thin (0.34 mm), 50-mm-diameter single crystal wafer of silicon coated with a 38-mm-diameter deposit of ^{6}LiF, fabricated at the Institute for Reference Materials and Measurements in Geel, Belgium. The manufacture of deposits and characterization of the ^{6}LiF areal density were exhaustively detailed in measurements performed over several years [13]. The average areal density was $\rho = (39.30 \pm 0.10)$ μg/cm^2. The α particles and tritons produced by the ^{6}Li$(n, t)^4$He reaction were detected by four surface barrier detectors, each with a well-defined and carefully measured solid angle. The geometry was chosen to make the solid angle subtended by the detectors insensitive to first order in the source position. The parameter ϵ_0 gives the ratio of detected alphas/tritons to incident thermal neutrons. It was calculated using

$$\epsilon_0 = \frac{\sigma_0}{4\pi} \iint \Omega(x, y)\rho(x, y)\theta(x, y)dxdy, \quad (5)$$

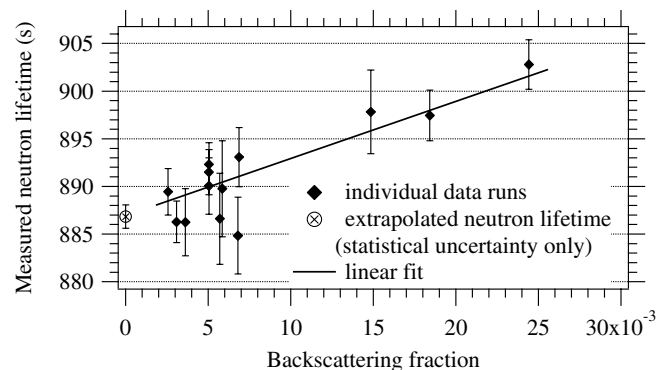where σ_0 is the cross section at thermal ($v_0 = 2200$ m/s)

FIG. 4.   A linear fit of the measured neutron lifetime at varying values of the detector backscattering fraction. The extrapolation to zero backscattering gives the free neutron lifetime.

TABLE I. Summary of systematic corrections and uncertainties (in seconds) for the measured neutron lifetime.

Source	Correction	Uncertainty
^{6}LiF foil areal density		2.2
^{6}Li cross section		1.2
Neutron detector solid angle	+1.5	1.0
Neutron beam halo	−1.0	1.0
LiF target thickness	+5.4	0.8
Trap nonlinearity	−5.3	0.8
Neutron losses in Si wafer	+1.3	0.5
^{6}LiF distribution in deposit	−1.7	0.1
Proton backscatter calc.		0.4
Proton counting statistics		1.2
Neutron counting statistics		0.1
Total	+0.2	3.4

velocity, $\Omega(x, y)$ is the detector solid angle, $\rho(x, y)$ is the areal mass density of the deposit, and $\theta(x, y)$ is the areal distribution of the neutron intensity on the target. The ^{6}Li thermal cross section is (941.0 ± 1.3) b [14]. It is important to note that we take the evaluated nuclear data files (ENDF/B-6) 1σ uncertainty from the evaluation, *not* the expanded uncertainty, to be the most appropriate for use with this precision experiment. The neutron detector solid angle was measured in two independent ways: mechanical contact metrology and calibration with ^{239}Pu alpha source of known absolute activity. These two methods agreed to within 0.1%.

The neutron beam intensity distribution was measured at both ends of the trap, and at the neutron monitor, using the Dy foil imaging technique [15]. This method provides almost five decades of dynamic range, making it ideal for sensitive neutron measurements. These quantitative images were used to determine the beam distribution function $\theta(x, y)$ in Eq. (5). We found that 0.1% of the neutron intensity is in the halo outside the effective radius of the proton detector.

Proton and neutron counting data were collected for 13 run series, each with a different proton detector and acceleration potential. The corrected value of the neutron lifetime for each series was calculated and plotted vs the backscattering fraction, as shown in Fig. 4. A linear extrapolation to zero backscattering gave a result of $\tau_n = (886.8 \pm 1.2[\text{stat}] \pm 3.2[\text{syst}])$ s. A summary of all corrections and uncertainties is given in Table I. This result would be improved by an independent absolute calibration of the neutron counter, which would significantly reduce the two largest systematic uncertainties, in the ^{6}LiF foil density and ^{6}Li cross section. A cryogenic neutron radiometer that promises to be capable of such a calibration at the 0.1% level has recently been demonstrated [16], and we are pursuing this method further. We expect that our experiment will ultimately achieve an uncertainty of less than 2 s.

[1] B. G. Yerozolimsky, Nucl. Instrum. Methods Phys. Res., Sect. A **440**, 491 (2000); H. Abele, Nucl. Instrum. Methods Phys. Res., Sect. A **440**, 499 (2000); H. Abele *et al.*, Phys. Rev. Lett. **88**, 211801 (2002); N. Severijns, Eur. Phys. J. A **15**, 217 (2002); I. S. Towner and J. C. Hardy, J. Phys. G **29**, 197 (2003).

[2] S. Burles, K. M. Nollett, J. W. Truran, and M. S. Turner, Phys. Rev. Lett. **82**, 4176 (1999); R. E. Lopez and M. S. Turner, Phys. Rev. D **59**, 103502 (1999).

[3] P. E. Spivak, Zh. Eksp. Teor. Fiz. **94**, 1 (1988).

[4] W. Mampe, P. Ageron, J. M. Pendlebury, and A. Steyerl, Phys. Rev. Lett. **63**, 593 (1989).

[5] W. Paul, F. Anton, L. Paul, S. Paul, and W. Mampe, Z. Phys. **45**, 25 (1989).

[6] V. V. Nezvizhevskii *et al.*, JETP **75**, 405 (1992).

[7] W. Mampe *et al.*, JETP Lett. **57**, 82 (1993).

[8] J. Byrne *et al.*, Europhys. Lett. **33**, 187 (1996).

[9] S. Arzumanov *et al.*, Phys. Lett. B **483**, 15 (2000).

[10] J. Byrne *et al.*, Nucl. Instrum. Methods Phys. Res., Sect. A **284**, 116 (1989); J. Byrne *et al.*, Phys. Rev. Lett. **65**, 289 (1990); A. P. Williams, Ph.D. thesis, University of Sussex, 1989 (unpublished); W. M. Snow *et al.*, Nucl. Instrum. Methods Phys. Res., Sect. A **440**, 528 (2000).

[11] A. A. Bergman and F. L. Shapiro, JETP **13**, 5 (1961).

[12] J. F. Ziegler, Stopping and Range of Ions in Matter (SRIM-2000), available at http://www.srim.org

[13] H. Tagziria *et al.*, Nucl. Instrum. Methods Phys. Res., Sect. A **303**, 123 (1991); J. Pauwels *et al.*, Nucl. Instrum. Methods Phys. Res., Sect. A **303**, 133 (1991); R. D. Scott *et al.*, Nucl. Instrum. Methods Phys. Res., Sect. A **314**, 163 (1992); J. Pauwels *et al.*, Nucl. Instrum. Methods Phys. Res., Sect. A **362**, 104 (1995); R. D. Scott *et al.*, Nucl. Instrum. Methods Phys. Res., Sect. A **362**, 151 (1995); J. Pauwels (private communication).

[14] A. D. Carlson *et al.*, U.S. government report, "The ENDF/B-VI Neutron Cross Sec. Measurement Standards," NISTIR 5177 (1993), available from NTIS (http://www.ntis.gov/).

[15] Z. Chowdhuri, Ph.D. thesis, Indiana University, 2000; Y. T. Cheng, T. Soodprasert, and J. M. R. Hutchinson, Appl. Radiat. Isot. **47**, 1023 (1996); Y. T. Cheng and D. F. R. Mildner, Nucl. Instrum. Methods Phys. Res., Sect. A **454**, 452 (2000).

[16] J. M. Richardson, W. M. Snow, Z. Chowdhuri, and G. L. Greene, IEEE Trans. Nucl. Sci. **45**, 550 (1998); Z. Chowdhuri *et al.*, Rev. Sci. Instrum. **74**, 4280 (2003).